Structural inhomogeneity and twinning in $YBa_2Cu_3O_{7-\delta}$ superconductors: High-resolution transmission electron microscopy measurements

Craig L. Johnson,* Jan K. Bording,† and Yimei Zhu
Brookhaven National Laboratory, Upton, New York 11973, USA
(Received 9 April 2008; published 18 July 2008)

The superconducting properties of $YBa_2Cu_3O_{7-\delta}$ (YBCO) are strongly dependent on atomic structure and composition. While the average structures of YBCO are well documented, the *local* oxygen concentration and ordering have received much less attention owing to the difficulty of experiments and analysis. We examined several samples of YBCO by quantitative high-resolution transmission electron microscopy and geometric phase analysis to determine their local atomic structure and symmetry. Our results reveal that adjacent domains separated by the (110) interfaces, commonly considered to be twin domains, can have different a_o/b_o ratios. The domains, therefore, do not retain the ideal twinned configuration commonly expected for this system. Assuming the a_o/b_o ratio is proportional to oxygen concentration, we suggest that these domains result from inhomogeneous oxygen distribution. Multiple measurements in both bulk and thin-film samples indicate that YBCO can consist of different phases, which may yield locally variable superconducting properties.

DOI: 10.1103/PhysRevB.78.014517 PACS number(s): 74.72.Bk, 68.37.Og, 61.72.Mm

I. INTRODUCTION

Microstructure and chemical composition profoundly affect the electronic properties of the high-temperature (high-T_c) superconductor $YBa_2Cu_3O_{7-\delta}$ (YBCO).[1] While the mechanisms behind type-II superconductivity in YBCO remain elusive, one necessary condition, upon which researchers agree, is that the CuO chain planes act as the charge reservoirs, and the charge carriers in the superconducting CuO_2 planes appear as a result of the electron transfer to the CuO chain planes. Thus, the local oxygen concentration and ordering in the CuO chain planes are vital for high-T_c superconductivity. For example, when the oxygen concentration changes from $\delta=0$ (fully oxygenated) to $\delta=0.65$, YBCO transforms from orthorhombic (Ortho I with $T_c=90$ K) and superconducting to tetragonal and nonsuperconducting. In addition, several intermediate phases with $T_c<90$ K are predicted to exist.[2–7] The simplest of these intermediates is the Ortho II phase with $\delta=0.5$. The atomic structures and stability of many of these phases have been examined, experimentally, by neutron and x-ray diffraction[8–18] and, theoretically, by density functional theory[7,19] and cluster-expansion calculations.[20–23]

The dominant microstructural feature in YBCO is twinning. Nevertheless, local structural inhomogeneity related to twin domains is not well known. As early as 1990, Joergensen *et al.*[24] observed a broadening of the neutron-diffraction Bragg peaks in oxygen-deficient YBCO. They suggested that this broadening might result from structural or compositional inhomogeneities. Structural inhomogeneities were also observed by electron microscopy.[25–33] While some of these electron-microscopy studies reported nanosized compositional domains,[25,26,28,29] others reported structural variations at the scale of the twin domain structure, ubiquitous in YBCO, and attributed these variations to inhomogeneities in the O concentration of the twin domains.[30,31,34] Electron-diffraction experiments also revealed local structural inhomogeneities. Beyers *et al.*[27] reported evidence that phase separation occurred in oxygen-deficient YBCO for narrow ranges of O content. Zhu *et al.*[32,33] observed diffraction patterns that showed evidence for 2a ordering, which is indicative of the Ortho II phase, in a YBCO sample with $\delta=0.1$. If the sample was compositionally and structurally homogenous, that stoichiometry would make the presence of the Ortho II phase impossible, whereas an inhomogenous sample could accommodate both the bulk composition and local 2a ordering.

In spite of these observations, YBCO is commonly considered to be homogenous in terms of chemical composition and oxygen ordering. Variations, if not simply overlooked, have been attributed to improper sample preparation and annealing. Here, we report a detailed study of several YBCO samples that exhibit compositional-structural variations on the nanoscale. We employed geometric phase analysis (GPA) to determine the local variations in orthorhombicity by analyzing the lattice-parameter ratios a_o/b_o in the (001) plane of YBCO. Our observations clearly show that YBCO can contain multiple structural phases even below a scale of 100 nm.

II. EXPERIMENTAL METHODS

Several samples of YBCO were examined using a JEOL 4000EX transmission electron microscope (operated at 400 keV; spherical-aberration coefficient 1.0 mm). Some of the samples have aged for as long as 10 years at room temperature in a desiccator. High-resolution transmission electron microscopy (HRTEM) images and diffraction patterns were collected on Fuji image plates and digitized using a 20-bit Ditabis Image Plate Reader. Transmission electron microscopy (TEM) specimens of bulk and thin-film YBCO were prepared with a standard ion milling procedure. We were careful to minimize possible beam damage during the sample preparation by low-voltage, low-angle and low-temperature milling. HRTEM images of YBCO grains in the [001] zone-axis orientation were studied using GPA.

GPA is an image-processing technique that analyzes the local Fourier components of the lattice fringes in a high-

resolution image. The local Fourier components $I_g(\mathbf{r})$ are obtained by filtering Fourier space for the desired **g** vector (reciprocal-lattice vector corresponding to a set lattice fringes in the image), and then calculating the inverse Fourier transform. The result is a real-space map of the information contained in the selected reflection and has both amplitude and phase components: $I_g(\mathbf{r})=A_g(\mathbf{r})\exp[iP_g(\mathbf{r})]$. The amplitude, $A_g(\mathbf{r})$, describes the local contrast of the lattice fringes, and the phase, $P_g(\mathbf{r})$, describes their positions. Information regarding the local lattice spacing is contained in $P_g(\mathbf{r})$. Accordingly, the phase is given by $P_g(\mathbf{r})=-2\pi\mathbf{g}\cdot\mathbf{u}(\mathbf{r})$, where $\mathbf{u}(\mathbf{r})$ is the displacement with respect to position. This result is identical to the phase component used in the Howie-Whelan equations to include dynamical scattering from a local lattice distortion.[35] The phase technique is commonly used to determine the displacements of lattice fringes in an image with respect to a reference lattice. A complete explanation of the local displacement determination by GPA is given by Hÿtch *et al.*[36]

Commonly, the reference area is a region of undeformed crystal away from the area of interest. In our study, we determined the reference lattice in multiple regions in the images and calculated the average a_o/b_o in those regions in the following way. First, the geometric phase maps of the (100) and (010) lattice fringes were determined. Subsequently, a large region within a single domain and containing no defects or imaging artifacts was selected, and the reference lattice (g^{ref}_{100} and g^{ref}_{010}) was determined. The a_o/b_o ratio for the selected area is given by $(g^{\mathrm{ref}}_{100}/g^{\mathrm{ref}}_{010})^{-1}$. In practice, **a** and **b** directions were not identified *a priori*, and a_o/b_o was taken to always be less than unity. In cases of images that were free of defects and imaging artifacts across most of the field of view, a_o/b_o was mapped to display the variation of a_o/b_o throughout the domains and across the domain interfaces.

When analyzing large fields of view [e.g., fields of view of negatives, image plates, or large charge-coupled device (CCD) cameras], artificial distortions from the microscope commonly obscure actual local variations in the image. The most significant artifact affecting GPA are the large-scale geometrical distortions, which increase with radial distance from the optical axis in the image plane of the microscope and are caused by the spherical aberrations of the projector-lens system. These projector-lens distortions are calibrated and removed following the method outlined by Hue *et al.*[37] The distortion correction allows quantitative analysis of our images of YBCO in which we compared data from different regions across the entire fields of view afforded by the image plates.

A second artifact that can occur when analyzing large fields of view results from thickness changes in the sample, which give rise to reduced contrast or contrast reversals in HRTEM images. Samples prepared for TEM analysis are commonly wedge shaped and, therefore, can have thickness changes across the field of view of an HRTEM image. Where contrast reduction occurs, the signal-to-noise ratio is greatly reduced, and the GPA results are not reliable. Contrast reversals often result in an apparent shift in the phase and an erroneous displacement. In both cases, the artifacts are obvious in the phase maps, and we avoided quantification of data from these regions of the images. In cases where thickness changes affect the image, we were careful only to compare regions of the image where the thickness is similar.

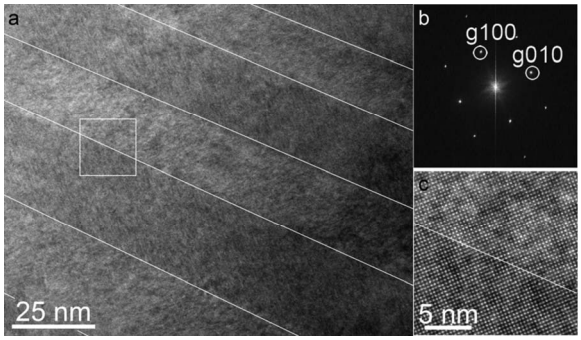

FIG. 1. HRTEM of YBCO thin film oriented with [001] parallel to the optical axis. (a) The white lines in the HRTEM image give the traces of the pseudotwin interfacial planes [parallel to (110)] separating the domains. (b) The digital diffractogram of the image in (a) shows the reflections g_{100} and g_{010} used for the geometric phase analysis. (c) The enlarged image of the boxed region from (a) shows the lattice fringe corresponding to the (100) and (010) crystallographic planes. The white line gives the trace of a domain boundary.

Finally, values of objective-lens defocus and specimen height were chosen to maximize the contrast of the lattice fringes. Maximization of the lattice-fringe contrast increases the signal-to-noise ratio and increases the likelihood of uniform contrast over large areas of the images. However, the global magnification in an image can change with experimental conditions such as defocus or specimen height. To avoid difficulties associated with uncertainties in magnification, we concentrated on the variations in lattice-parameter ratios rather than the absolute values of a_o and b_o.

III. RESULTS AND DISCUSSIONS

HRTEM images (Fig. 1) exhibit the common twinned microstructure of YBCO with domains parallel to (110) and related by a nearly 90° rotation of the (100) and (010) lattice planes about the [001] axis across the interfaces. Although the interfaces in Fig. 1 produce only diffuse contrast, which is typical for twin boundaries in not fully oxygenated YBCO samples, the fast Fourier transform (FFT) of the image clearly shows the splitting of the *hh*0 diffraction spots, suggesting the rotation of the (100) and (010) lattice planes.

Using the procedure outlined above, we determined the local a_o/b_o from Fig. 1(a). The resulting a_o/b_o map [Fig. 2(a)] clearly shows the structural change that occurs across the twin boundaries. Furthermore, we quantified the changes in a_o/b_o by analyzing profiles like the one in Fig. 2(b). The profile shows that in domains D1, D3, and D5, the average a_o/b_o is 0.996, while in the adjacent domains, D2 and D4, a_o/b_o is 0.983.

The atomic arrangements on either side of an ideal twin boundary are identical and related by a plane of mirror symmetry coincident with the interface. Consequently, the magnitude of a_o/b_o must remain constant across the boundary. The values of a_o/b_o determined from Fig. 1 differ from do-

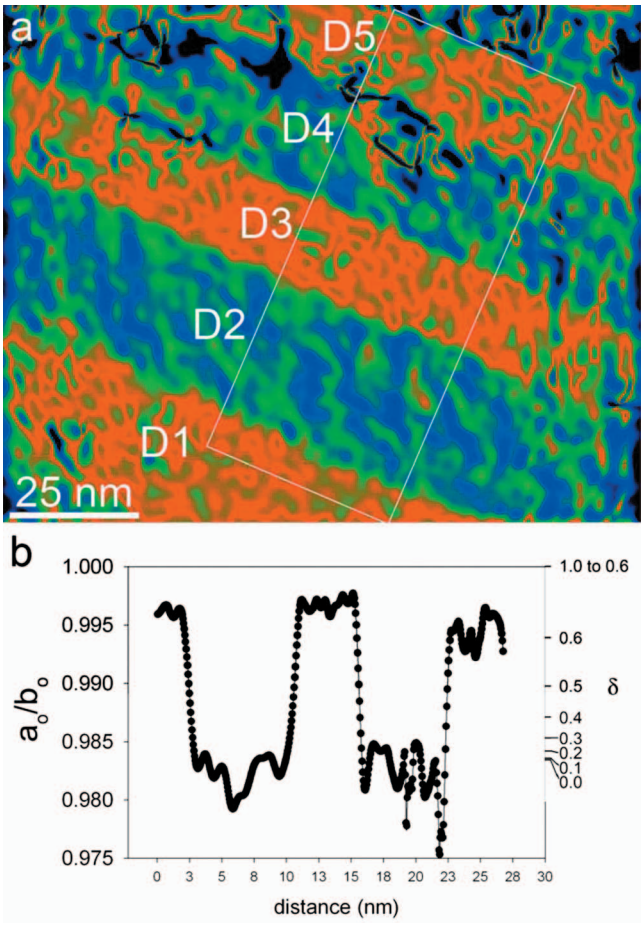

FIG. 2. (Color) Local a_o/b_o ratio for thin-film sample of YBCO. (a) Map of a_o/b_o values from the HRTEM image in Fig. 1(a) shows the oscillations of a_o/b_o ratio from domain to domain. The domains in red (D1, D3, and D5) have $a_o/b_o \sim 0.996$, while the adjacent domains in blue (D2 and D4) have $a_o/b_o \sim 0.983$. (b) The graph shows the values of a_o/b_o across the domains perpendicular to the interfaces along the length of the boxed region and averaged over its width. In this case the values of a_o/b_o are consistent with alternating Ortho I (D2 and D4) and Ortho II (D1, D3, and D5) domains. The scale on the right of the plot gives the corresponding δ values determined from the plot in Ref. 28 (Ref. 48).

main to domain; therefore, the adjacent domains are not strictly twins. These boundaries, however, share some of the features of true (110) twin boundaries in YBCO, i.e., the relationship between the domains involves a *nearly* 90° lattice rotation [i.e., (100) lattice planes become (010) and vice versa], and the interface is in the (110) plane. Hence, we refer to the boundaries that separate two domains with different a_o/b_o as pseudotwin boundaries.

We applied similar analysis to domains from several YBCO samples. In the samples analyzed, adjacent domains commonly have significantly different a_o/b_o. Figure 3 shows three examples. In the first image [Fig. 3(a)], the center domain has $a_o/b_o=0.987$ while the two adjacent domains are tetragonal ($a_o/b_o=1$). The second image [Fig. 3(b)] shows a similar case with $a_o/b_o=0.988$ and 0.996 for adjacent domains. However, in the third image [Fig. 3(c)], the a_o/b_o (0.992) remains constant across the boundary.

The results of the analyses are presented in the bar graph in Fig. 4. In the plot, measurements are grouped, first, by image, i.e., the measurements taken from a single HRTEM image are assigned a number and grouped side by side. Multiple images from the same YBCO grain are labeled with capital letters. In most images, we observed at least two distinct values of a_o/b_o. For multiple images taken from the same sample, the a_o/b_o also tends toward two values. Furthermore, the differences between a_o/b_o commonly oscillate from high to low values from one domain to the next within a single grain. The a_o/b_o ratios we measured from our samples span the full range of possible values as found by neutron diffraction ($0.983 < a_o/b_o \leq 1$), including the tetragonal phase. Domains separated by the pseudotwin boundaries in the thin-film sample (e.g., domains in Fig. 2; Data 4 and 5 in Fig. 4) have a_o/b_o ratios consistent with the most common O-ordered phases (Ortho I: $a_o/b_o \sim 0.983$ and Ortho II: $a_o/b_o \sim 0.995$), and these domains oscillate from high to low a_o/b_o (i.e., OI↔OII↔OI). The bulk samples (Data 1 to 3 and 6 to 13 in Fig. 4) exhibit the same a_o/b_o oscillation, but the measured a_o/b_o do not necessarily match those expected for the Ortho I or Ortho II phases. The tetragonal phase is present in some of the bulk samples we examined. Finally, within the measured area of the domains, a_o/b_o is constant over distances much longer than the domain width.

These data are supported by electron-diffraction measurements. Selected-area electron diffraction (SAED) patterns from areas containing sets of parallel domains exhibit asymmetric splitting of 110 reflections (e.g., Fig. 5), i.e., different a_o/b_o. The asymmetry of the splitting confirms the structural inhomogeneity among the domains. The sharp, rather than smeared reflections indicate that discrete values of a_o/b_o occur in this sample rather than a range of values as would be expected if the material were inhomogeneous on an even smaller scale. In some samples, across a few twin domains using SAED at high-order reflections, we observed the $hh0$ spots split into more than three spots, which suggests a local variation in orthorhombicity. The angular distance (θ_{110}) of the spots from a line perpendicular to the line through the orthogonal set of 110 reflections (not split) θ_{110} can be used to estimate a_o/b_o using the relationship: $a_o/b_o = \tan[(-\theta_{110} + \pi)/4]$. However, this method is rather insensitive, as a result of the small splitting angles, and provides no access to spatial distributions of the phases.

Assuming a direct relationship between the structure and composition, we can infer the local oxygen content in the sample from our a_o/b_o data. Neutron-diffraction studies established that the lattice parameters a_o and b_o change systematically with O content (Fig. 6). In samples with $\delta=0$, the structure is orthorhombic with $a_o/b_o \sim 0.983$. As δ increases (O content decreases), the a_o/b_o ratio decreases until $\delta = \sim 0.65$ at which point the structure is tetragonal (i.e., $a=b$) and not superconducting. Applying this relationship to the data from Fig. 2, for example, we can infer that domains D2 and D4 have a_o/b_o consistent with fully oxygenated, superconducting YBCO, while adjacent domains (D1, D3, and D5) have a_o/b_o consistent with the oxygen-deficient Ortho-II phase. However, this relationship was determined from average values of a_o/b_o ratios from large volumes of YBCO,

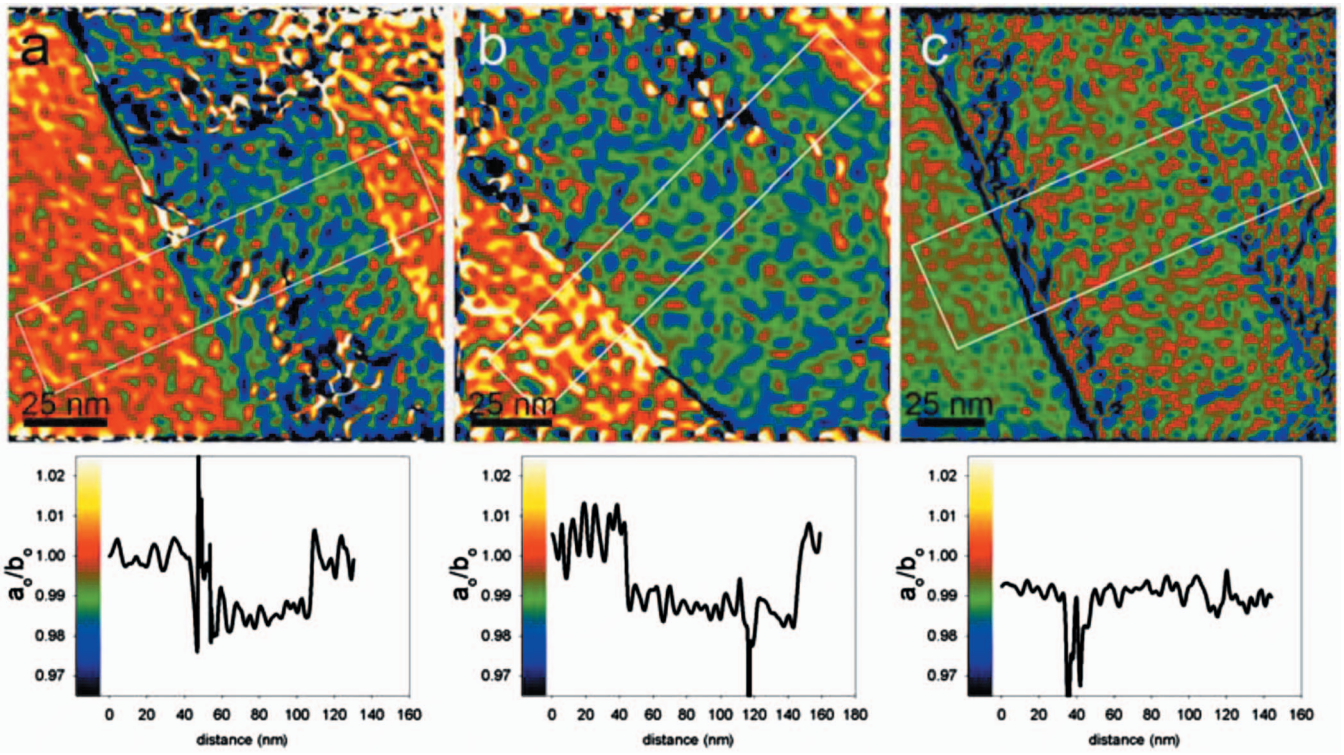

FIG. 3. (Color) Local a_o/b_o maps and corresponding profiles for three samples of YBCO. The maps of a_o/b_o from two different bulk-YBCO samples show that the structures can oscillate (a) between tetragonal ($a_o/b_o=1$) and orthorhombic ($a_o/b_o=0.988$), (b) between two different orthorhombic values [$a_o/b_o=0.988$ (center domain) and 0.996 (inversion of the value (1.004) determined from the profile)], and across the domain interfaces. (c) The map shows the a_o/b_o from a bulk sample with nearly perfect twin boundaries, i.e., the a_o/b_o remains constant (0.992) across the domain boundaries. Scale bars in the images are 25 nm.

while, in this work, we stress the existence of varying a_o/b_o on a local scale. Therefore, the local O concentrations inferred from this relationship should be viewed as estimates.

Our data reveal three important structural features that occur in YBCO samples: (1) the a_o/b_o and, by extension, the O content in adjacent domains can be different, which excludes them from being true twin domains, (2) while the thin-film samples have a_o/b_o consistent with the well-ordered Ortho I and Ortho II phases, the full range of a_o/b_o, including the tetragonal phase, are represented in our data set, and (3) that single grains commonly contain no more than two phases with the a_o/b_o oscillating between high and low values from domain to domain. These observations have considerable implications for superconductivity in YBCO.

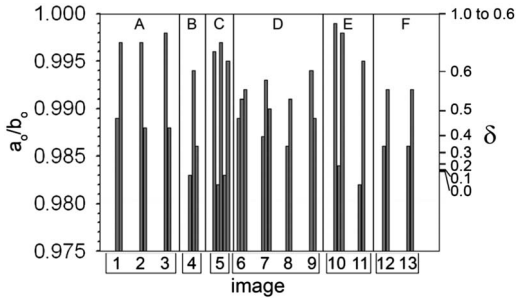

FIG. 4. Graph of a_o/b_o ratios measured from individual domains in our samples. The measurements are grouped by image (given by the number) and by sample (images taken from the same grain/sample are boxed together and labeled with a capital letter). For example, the a_o/b_o ratios corresponding to the number "1" are from two adjacent domains in a single image, and images 1, 2, and 3 all come from the same grain (a) in one sample. The scale on the right side of the graph gives the value of δ in $YBa_2Cu_3O_{7-\delta}$ as inferred from neutron-diffraction data (Ref. 48).

Oscillation from orthorhombic to tetragonal, or between various O concentrations, implies an oscillation between superconducting and nonsuperconducting domains. Extrapolating to large-scale samples, these oscillating domains could form channels or a percolation network of superconducting material in a nonsuperconducting matrix. Such a network would result in unexpected and interesting properties and may explain some anomalous observations. Surprisingly strong flux pinning and a temperature-dependent fishtail have already been used to infer the existence of weak or nonsuperconducting regions in YBCO.[38,39] Because these regions were not directly observed, researchers suggested that twin boundaries trapped flux vortices and increased critical current densities.[38–40] Observations that a stronger fishtail effect occurred for samples with lower O content and higher densities of twin boundaries and that the fishtail effect was reduced in samples with low twin-boundary density were both consistent with that conclusion.[41] In light of our observations, we suggest a slightly different explanation. In samples with less than optimal O concentration, twins signal the existence of domains with varying degree of oxygenation and different T_c, sometimes even $T_c=0$ K. The resulting small nonsuperconducting regions provide an explanation for the

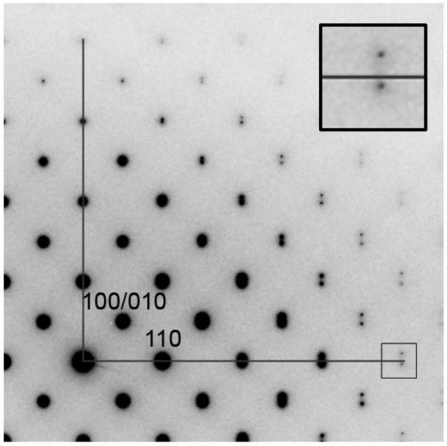

FIG. 5. Selected-area electron diffraction pattern of YBCO in [001] zone-axis orientation. The diffraction pattern is taken from an area containing a few parallel twin domains, similar to Fig. 2 with two distinct a_o/b_o ratios. Owing to the twinning structure of YBCO, one set of 110 reflections is split, while the reflections from the perpendicular set remain singular. The vertical line is drawn through the centers of the unsplit 1–10 reflections, and the horizontal line is exactly perpendicular to that one. The splitting of the 110 reflections, in this case, is asymmetric (with respect to the horizontal line), which indicates different a_o/b_o ratios in the selected area. Diffraction patterns obtained from the YBCO samples we examined commonly show similar asymmetric splitting, which corroborates the real-space determinations of inhomogeneous a_o/b_o.

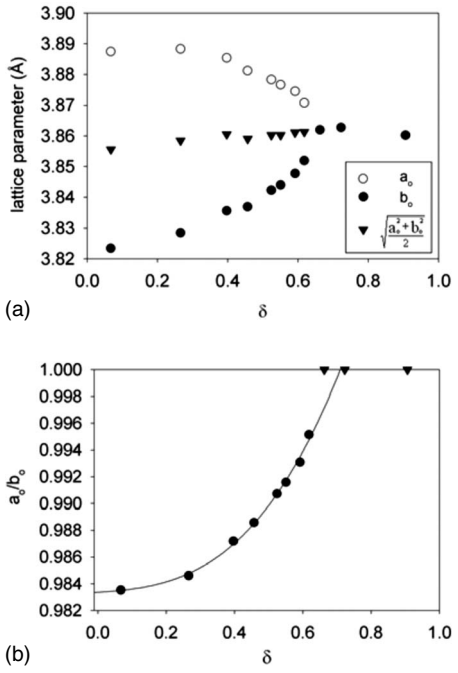

FIG. 6. Relationships of O concentration to the lattice parameters and a_o/b_o ratio of YBCO. (a) Graph of lattice parameters a_o (open circles) and b_o (filled circles) and $\sqrt{(a^2+b^2)}/2$ vs δ from the neutron-diffraction data of Jorgensen *et al.* (Ref. 48). The shallow slope of the $\sqrt{(a^2+b^2)}/2$ data indicates that the (110) spacing remains nearly constant throughout the phase changes, suggesting that even a pseudotwin is a low energy interface in YBCO. (b) Relationship of a_o/b_o ratio to δ. Triangles represent samples with values of $\delta > 0.65$, all of which have the tetragonal structure. YBCO with δ between 0 and 0.65 (dots) are orthorhombic and superconducting. From this curve the local oxygen content in our YBCO samples was inferred from measured local a_o/b_o ratios.

temperature-dependent fishtail effect, in that they reduce vortex mobility.

The origin of the oscillating two-phase regions we detected is difficult to determine. All the YBCO samples we studied were sintered at high temperature (>700 °C; YBCO, regardless of oxygen content, is tetragonal above ~665 °C) followed by cooling in a controlled oxygen atmosphere. During cooling, the YBCO transforms from the tetragonal phase to various orthorhombic phases if δ remains less than 0.65. Twinning in YBCO results from strain induced by this tetragonal-to-orthorhombic transition of a crystal confined within a matrix. For example, the T-O transition for a perfectly crystalline cube-shaped grain suspended in vacuum would result in a shape change to a perfectly crystalline rectangular block. As the transformation takes place in bulk and thin-film YBCO, an internal strain results because the grains are confined by surrounding grains, and the shape change is restricted. Twins form on (110) planes to relax this strain and minimize shape change. Irregular-shaped grains in real YBCO samples ensure that normal twinning will not completely relax the strain generated by the transition. Therefore, a residual strain within the domains can be reasonably expected. The T-O transition occurs around 665 °C. However, below this temperature, the O diffusivity remains high.[42] Indeed, O diffusion has been reported to occur even at room temperature.[43–46] Therefore, the O composition could redistribute among the twin domains resulting in pseudotwins such as we observed. Such strain-induced spinodal decomposition may occur when stresses resulting from confinement are above a critical value. In this scenario, the YBCO would lower its total energy by shifting O across the twin boundaries to obtain the most favorable a_o/b_o ratios and forming the pseudotwins. The oscillation of a_o/b_o ratio from domain to domain is consistent with the conclusion of Katchaturyan and Morris[5] that YBCO undergoes spinodal decomposition into phases with different O concentrations; however, we suggest that this decomposition may be activated, at least in part, by strain rather than by a miscibility gap. The occurrence of stoichiometric phases in the thin-film samples, compared to the multitude of phases in the bulk samples, may support this conclusion. An alternative scenario is that, in order to relax interfacial strain or confinement strain, adjacent domains lose oxygen to the atmosphere at a differential rate resulting in the observed oscillating structure. Furthermore, the wide range of a_o/b_o we observed is not surprising since HRTEM only measures the average structure projected through the thickness of the sample. Our measurements (Fig. 4) focus on a_o/b_o ratio at the scale of domain width, which is on the same order as the sample thickness and do not exclude the possibility that, in some cases, oxygen related inhomogeneity occurs at a scale much smaller than the domain width.[47]

The point we want to make here is that the real *local* structure in YBCO is significantly deviated from the ideal one that is commonly accepted by our research community

and described in literature. Based on our present work, for most of the YBCO samples, including those with oxygen deficiency or slight deficiency ($\delta \ll 0.1$), as well as fully oxygenated but aged for a long period of time even at room temperature under a dry atmosphere, the twinning structure with a mirror symmetry plane and identical a_o/b_o ratios and composition across the interfaces can no longer be assumed. Most importantly, superconducting properties in these samples are likely to be considerably different from domain to domain as a result of local structural inhomogeneity. One can easily imagine a material, in that case, with superconducting percolation networks in a nonsuperconducting matrix. Indeed, such a network could have profound implications for theories of pinning and magnetic flux in YBCO. We are currently developing tight-binding calculations to simulate YBCO behavior using many-atom models. These calculations may allow us to check the explanations offered here for the variation in O content and, furthermore, allow us to examine the electronic properties of such inhomogeneous YBCO pseudotwin microstructures.

ACKNOWLEDGMENT

The work at BNL was supported by the U.S. Department of Energy, Division of Materials Science, Office of Basic Energy Science, under Contract No. DE-AC02-98CH10886.

*Present address: CEMES-CNRS, 29, rue Jeanne-Marvig, Toulouse 31055,Cedex, France.

†Present address: University of Stavanger, Stavanger NO-4036, Norway.

[1] Z.-X. Cai and Y. Zhu, *Microstructures and Structural Defects in High-Temperature Superconductors* (World Scientific, Singapore, 1998).

[2] A. G. Khachaturyan, S. V. Semenovskaya, and J. W. Morris, Phys. Rev. B **37**, 2243 (1988).

[3] A. G. Khachaturyan and J. W. Morris, Phys. Rev. Lett. **64**, 76 (1990).

[4] A. G. Khachaturyan and J. W. Morris, Phys. Rev. Lett. **61**, 215 (1988).

[5] A. G. Khachaturyan and J. W. Morris, Phys. Rev. Lett. **59**, 2776 (1987).

[6] D. de Fontaine, V. Ozolins, Z. Islam, and S. C. Moss Phys. Rev. B **71**, 212504 (2005).

[7] D. de Fontaine, G. Ceder, and M. Asta, Nature (London) **343**, 544 (1990).

[8] N. H. Andersen, M. von Zimmermann, T. Frello, M. Kall, D. Monster, P. A. Lindgard, J. Madsen, T. Niemoller, H. F. Poulsen, O. Schmidt, J. R. Schneider, T. Wolf, P. Dosanjh, and W. N. Hardy, Physica C **317**, 259 (1999).

[9] H. F. Poulsen, M. von Zimmermann, J. R. Schneider, N. H. Andersen, P. Schleger, J. Madsen, R. Hadfield, H. Casalta, R. X. Liang, P. Dosanjh, and W. N. Hardy, Phys. Rev. B **53**, 15335 (1996).

[10] P. Schleger, H. Casalta, R. Hadfield, H. F. Poulsen, M. von Zimmermann, N. H. Andersen, J. R. Schneider, R. X. Liang, P. Dosanjh, and W. N. Hardy, Physica C **241**, 103 (1995).

[11] P. Schleger, R. A. Hadfield, H. Casalta, N. H. Andersen, H. F. Poulsen, M. von Zimmermann, J. R. Schneider, R. X. Liang, P. Dosanjh, and W. N. Hardy, Phys. Rev. Lett. **74**, 1446 (1995).

[12] W. Schwarz, O. Blaschko, G. Collin, and F. Marucco, Phys. Rev. B **48**, 6513 (1993).

[13] R. Sonntag, D. Hohlwein, T. Bruckel, and G. Collin, Phys. Rev. Lett. **66**, 1497 (1991).

[14] R. M. Fleming, L. F. Schneemeyer, P. K. Gallagher, B. Batlogg, L. W. Rupp, and J. V. Waszczak, Phys. Rev. B **37**, 7920 (1988).

[15] J. Grybos, D. Hohlwein, T. Zeiske, R. Sonntag, F. Kubanek, K. Eichhornand, and T. Wolf, Physica C **220**, 138 (1994).

[16] R. X. Liang, D. A. Bonn, and W. N. Hardy, Physica C **336**, 57 (2000).

[17] V. Plakhty, A. Stratilatov, Y. Chernenkov, V. Fedorov, S. K. Sinha, C. K. Loong, B. Gaulin, M. Vlasov, and S. Moshkin, Solid State Commun. **84**, 639 (1992).

[18] A. Stratilatov, V. Plakhty, Y. Chernenkov, and V. Fedorov, Phys. Lett. A **180**, 137 (1993).

[19] W. E. Pickett, Rev. Mod. Phys. **61**, 433 (1989).

[20] G. Ceder, M. Asta, W. C. Carter, M. Kraitchman, D. de Fontaine, M. E. Mann, and M. Sluiter, Phys. Rev. B **41**, 8698 (1990).

[21] G. Ceder, M. Asta, and D. de Fontaine, Physica C **177**, 106 (1991).

[22] D. de Fontaine, L. T. Wille, and S. C. Moss, Phys. Rev. B **36**, 5709 (1987).

[23] D. Monster, P. A. Lindgard, and N. H. Andersen Phys. Rev. B **64**, 224520 (2001).

[24] J. D. Jorgensen, B. W. Veal, A. P. Paulikas, L. J. Nowicki, G. W. Crabtree, H. Claus, and W. K. Kwok, Phys. Rev. B **41**, 1863 (1990).

[25] J. C. Barry, J. Electron Microsc. Tech. **8**, 325 (1988).

[26] J. C. Barry and J. A. Alarco, J. Microsc. **202**, 495 (2001).

[27] R. Beyers, B. T. Ahn, G. Gorman, V. Y. Lee, S. S. P. Parkin, M. L. Ramirez, K. P. Roche, J. E. Vazquez, T. M. Gur, and R. A. Huggins, Nature (London) **340**, 619 (1989).

[28] J. Etheridge, Philos. Mag. A **73**, 643 (1996).

[29] M. Sarikaya and E. A. Stern, Phys. Rev. B **37**, 9373 (1988).

[30] E. J. Williams and W. M. Stobbs, Philos. Mag. A **68**, 1 (1993).

[31] Y. Yan, W. Y. Liang, T. Walther, and W. M. Stobbs, Phys. Rev. B **54**, 16234 (1996).

[32] Y. Zhu, A. R. Moodenbaugh, M. Suenaga, and J. Tafto, Physica C **167**, 363 (1990).

[33] Y. M. Zhu, M. Suenaga, J. Tafto, and D. O. Welch, Phys. Rev. B **44**, 2871 (1991).

[34] P. A. Midgley, R. Vincent, and D. Cherns, Philos. Mag. A **66**, 237 (1992).

[35] P. B. Hirsch, A. Howie, and M. J. Whelan, Philos. Trans. R. Soc. London, Ser. A **252**, 499 (1960).

[36] M. J. Hytch, E. Snoeck, and R. Kilaas, Ultramicroscopy **74**, 131 (1998).

[37] F. Hüe, C. L. Johnson, S. Lartigue-Korinek, G. Wang, P. R. Buseck, and M. J. Hÿtch, J. Electron Microsc. **54**, 181 (2005).

[38] A. A. Zhukov, H. Kupfer, H. Claus, H. Wuhl, M. Klaser, and G. Muller-Vogt, Phys. Rev. B **52**, R9871 (1995).

[39] M. Daeumling, J. M. Seuntjens, and D. C. Larbalestier, Nature (London) **346**, 332 (1990).
[40] P. Degroot, C. Beduz, Z. A. Yi, Z. A. Yi, R. Yanru, and S. Smith, Physica C **185**, 2471 (1991).
[41] J. Shibata, T. Honjo, H. Fuji, T. Araki, I. Hirabayashi, T. Izumi, Y. Shiohara, T. Yamamoto, and Y. Ikuhara, J. Mater. Res. **17**, 1266 (2002).
[42] K. N. Tu, S. I. Park, and C. C. Tsuei, Appl. Phys. Lett. **51**, 2158 (1987).
[43] J. D. Jorgensen, S. Pei, P. Lightfoot, H. Shi, A. P. Paulikas, and B. W. Veal, Physica C **167**, 571 (1990).
[44] B. W. Veal, H. You, A. P. Paulikas, H. Shi, Y. Fang, and J. W. Downey, Phys. Rev. B **42**, 4770 (1990).
[45] R. Mogilevsky, R. Levi-Setti, B. Pashmakov, L. Liu, K. Zhang, H. M. Jaeger, D. B. Buchholz, R. P. H. Chang, and B. W. Veal, Phys. Rev. B **49**, 6420 (1994).
[46] I. Poberaj, D. Mihailovic, and S. Bernik, Phys. Rev. B **42**, 393 (1990).
[47] Q. P. Meng and Y. M. Zhu Phys. Rev. B **75**, 174501 (2007).
[48] J. D. Jorgensen, B. W. Veal, W. K. Kwok, G. W. Crabtree, A. Umezawa, L. J. Nowicki, and A. P. Paulikas, Phys. Rev. B **36**, 5731 (1987).